Electronic Supplementary Material (ESI) for Inorganic Chemistry Frontiers.

Electronic Supplementary Information

Inert Macrocyclic Eu^{3+} Complex with Affirmative paraCEST Features

Tanja Gambino,[a] Laura Valencia,[b] Paulo Pérez-Lourido,[b] David Esteban-Gómez,[c] Moritz Zaiss,[d] Carlos Platas-Iglesias*[c] and Goran Angelovski*[a]

[a] MR Neuroimaging Agents, MPI for Biological Cybernetics, Tuebingen Germany.
Email: goran.angelovski@tuebingen.mpg.de

[b] Departamento de Química Inorgánica, Facultad de Ciencias, Universidade de Vigo, As Lagoas, Marcosende, 36310 Pontevedra, Spain.

[c] Centro de Investigacións Científicas Avanzadas (CICA) and Departamento de Química, Facultade de Ciencias, Universidade da Coruña, 15071 A Coruña Spain.
Email: carlos.platas.iglesias@udc.es

[d] High-Field Magnetic Resonance, MPI for Biological Cybernetics, Tuebingen, Germany.

Table of Contents

Supplementary Figures

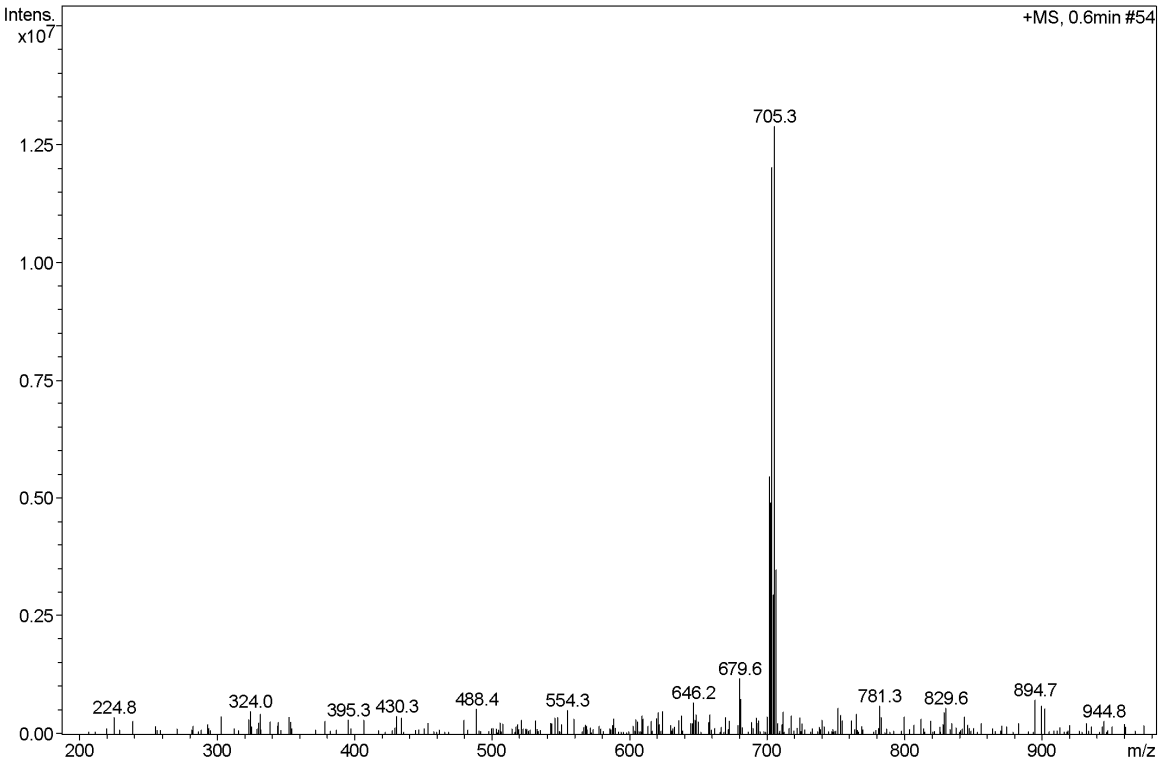

Figure S1. ESI-MS spectrum of the [**Eu(L-2H)**]$^{+}$.

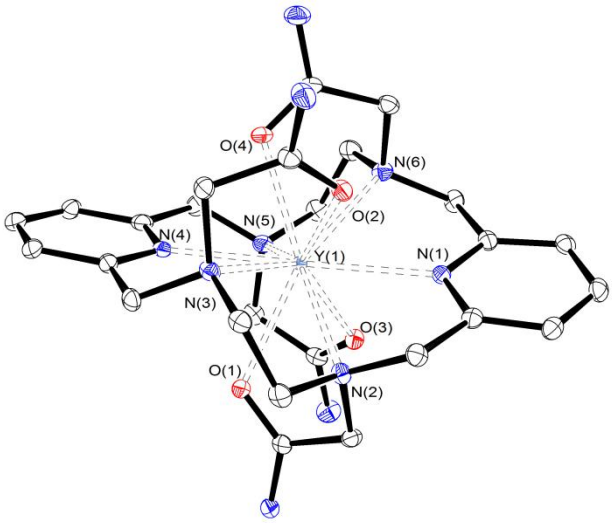

Figure S2. View of the structure of the $[\mathbf{YL}]^{3+}$ cation present in crystals of $[\mathbf{YL}](NO_3)_3 \cdot 3H_2O$. Hydrogen atoms are omitted for simplicity.

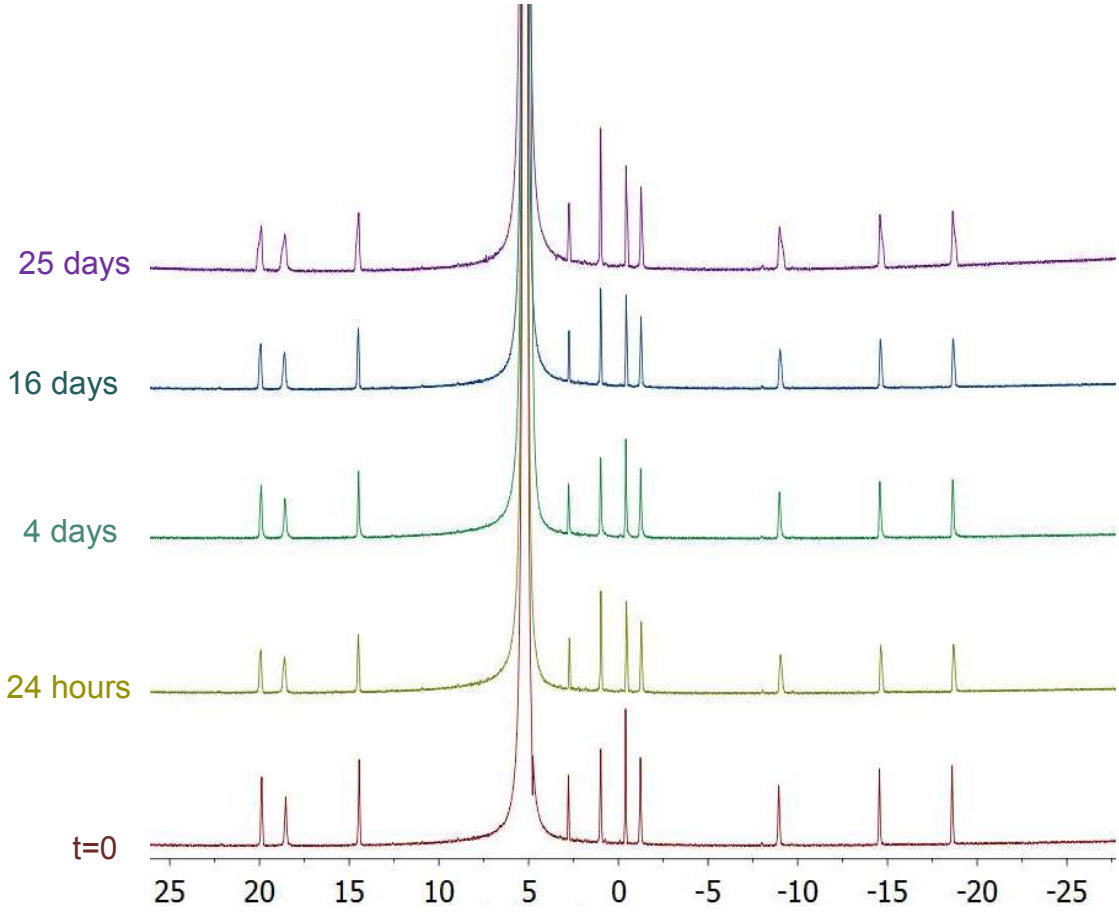

Figure S3. ^{1}H NMR spectra (400 MHz) of **EuL** recorded in 1 M HCl at 25 ºC over time.

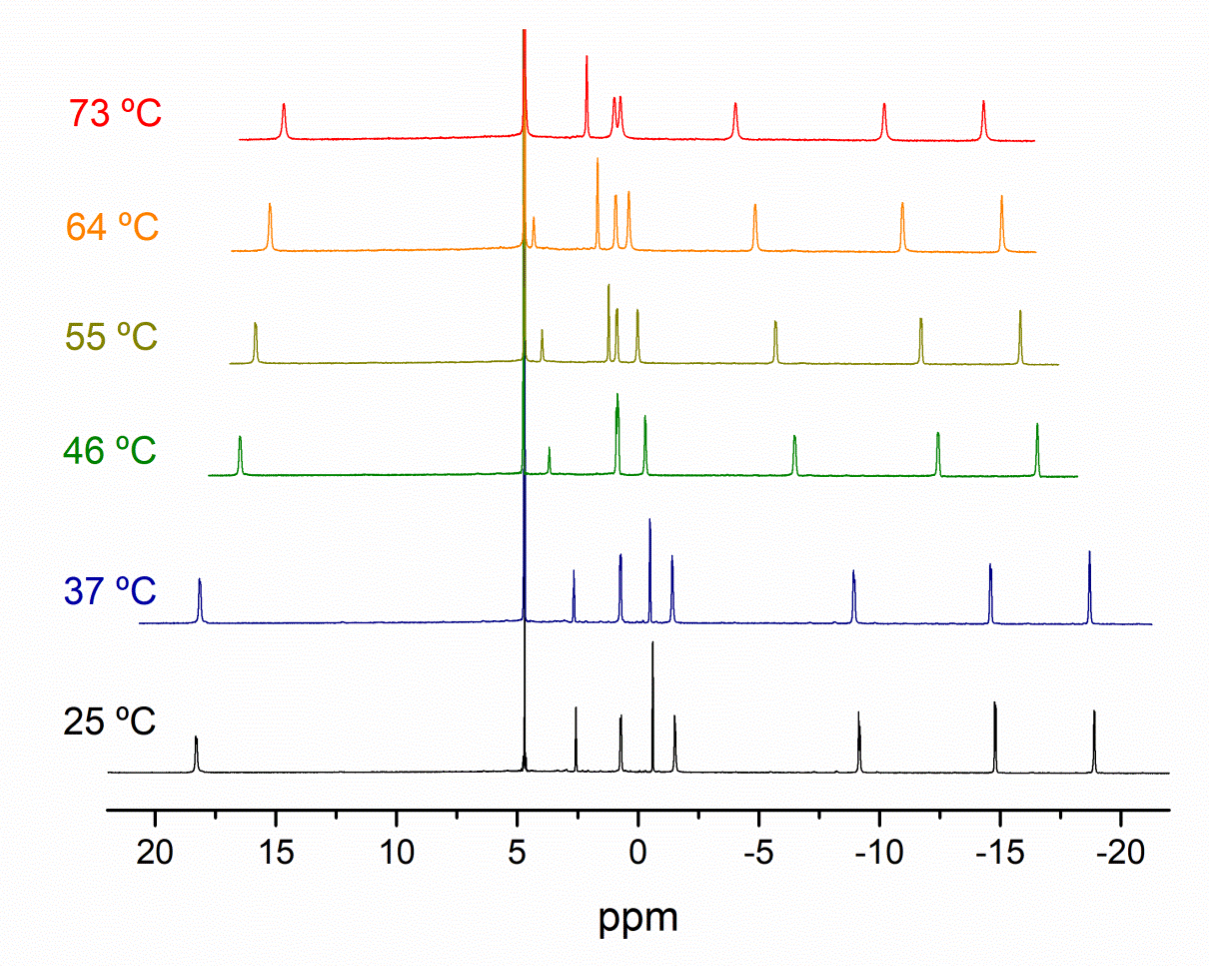

Figure S4. ^{1}H NMR spectra of **EuL** (5 mM, pH 7.0, 1 equiv. Zn^{2+}, phosphate buffer, $[NaH_2PO_4]$ = 0.026 M; $[Na_2HPO_4]$ = 0.041 M) recorded at different temperatures.

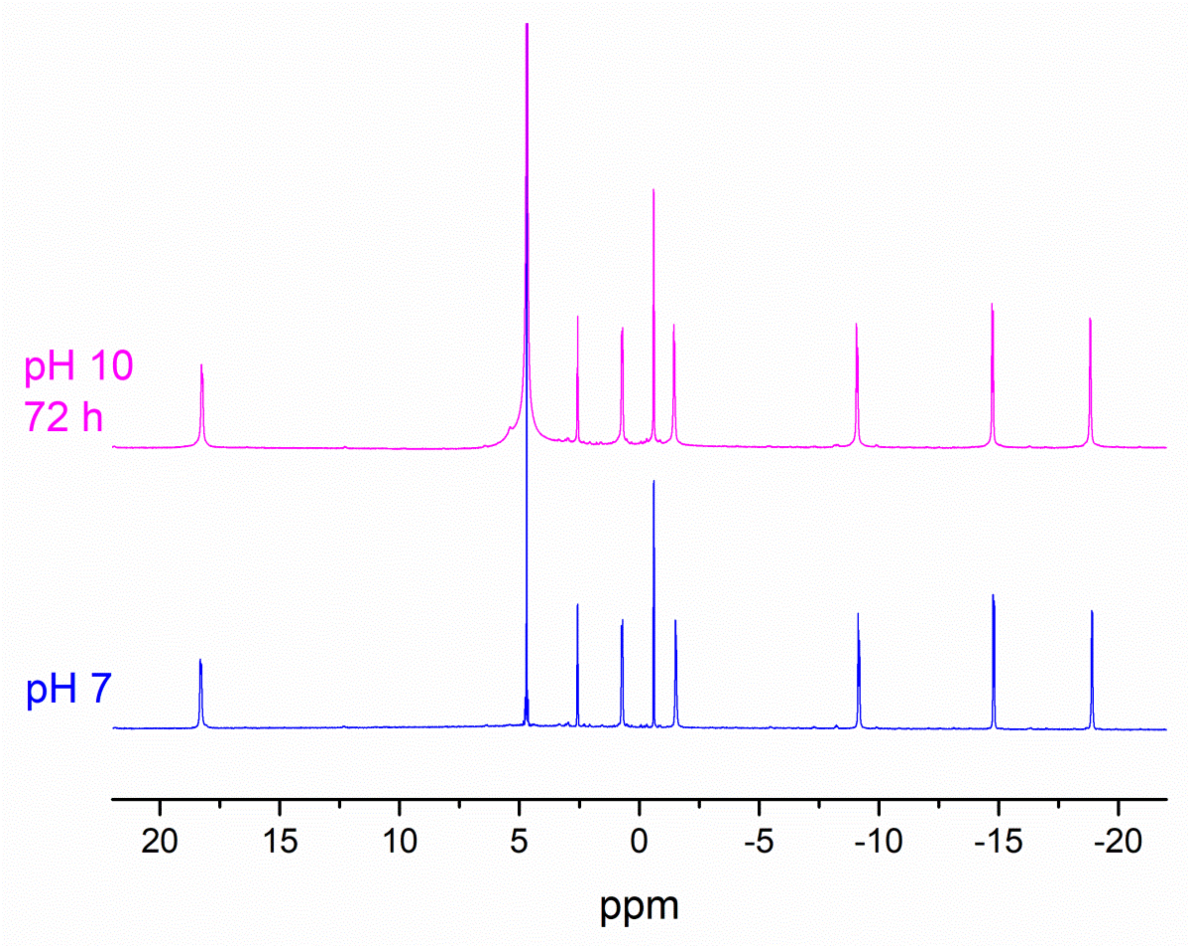

Figure S5. ^{1}H NMR spectra of **EuL** (25 ºC, 15 mM) recorded at different pH values.

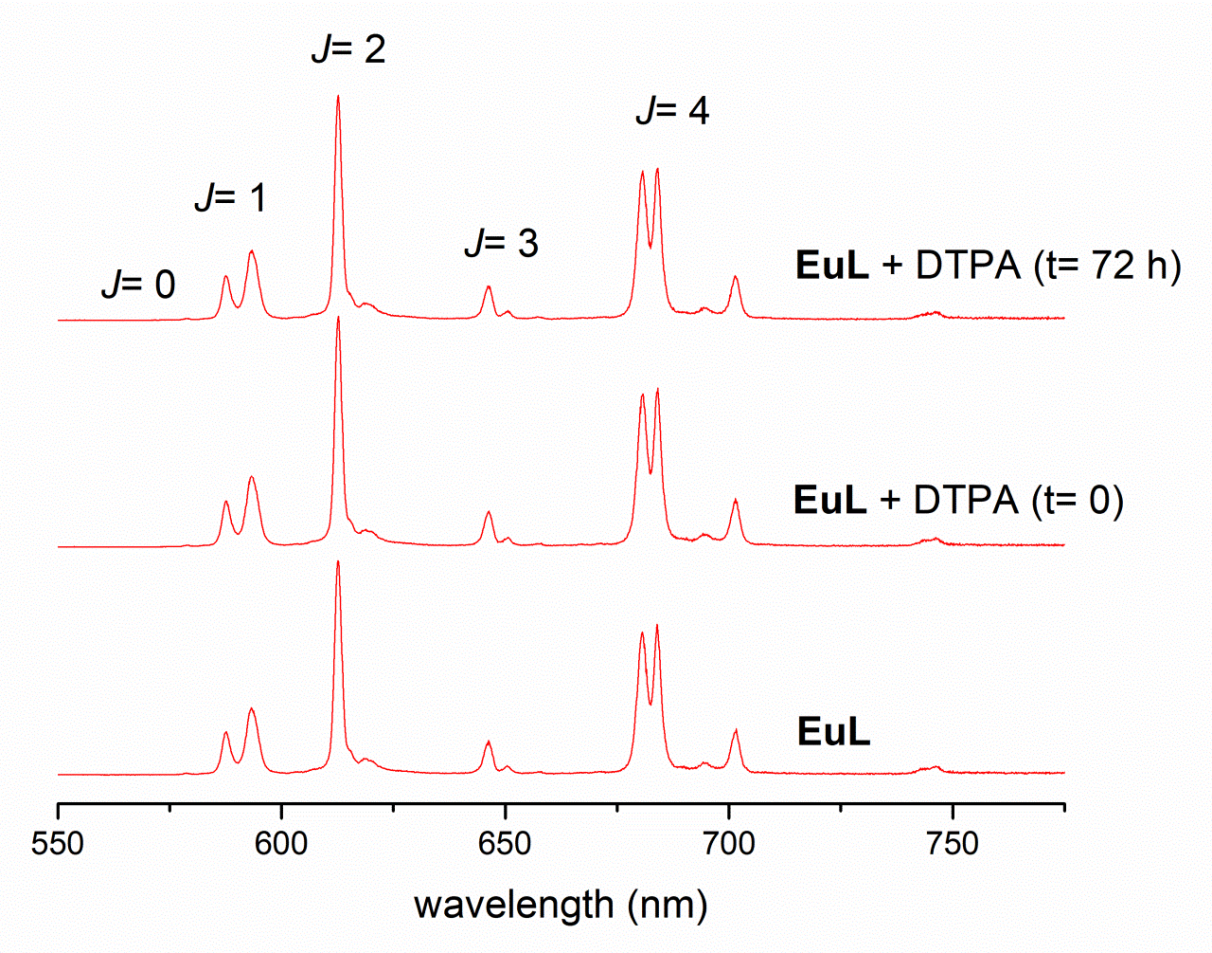

Figure S6. Emission spectra of **EuL** (5×10^{-5} M, pH 7.0, phosphate buffer, [NaH_2PO_4] = 0.026 M; [Na_2HPO_4] = 0.041 M, 25 ºC) recorded before and after addition of ten equivalents of DTPA.

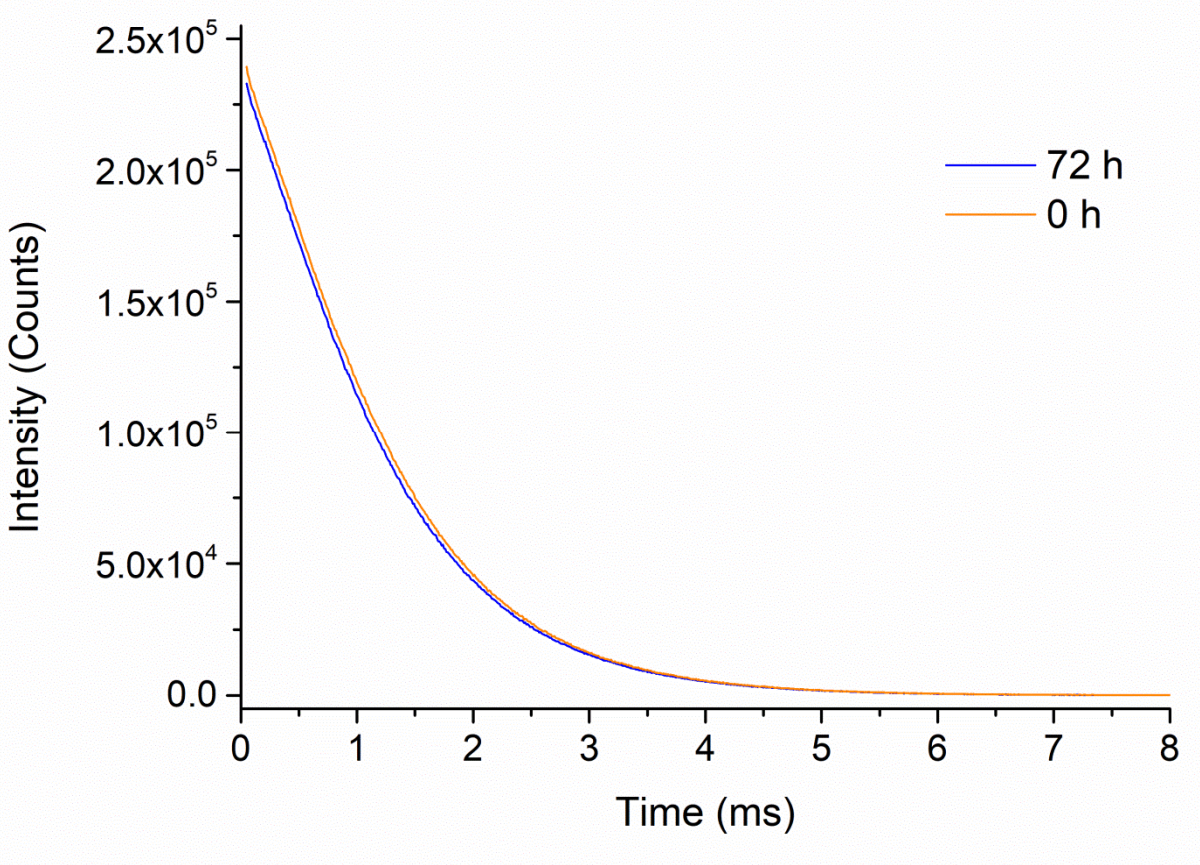

Figure S7. Phosphorescence decay curves of **EuL** (5×10^{-5} M, pH 7.0, phosphate buffer, $[NaH_2PO_4]$ = 0.026 M; $[Na_2HPO_4]$ = 0.041 M, 25 ºC) recorded before (0 h) and 72 h after addition of ten equivalents of DTPA.

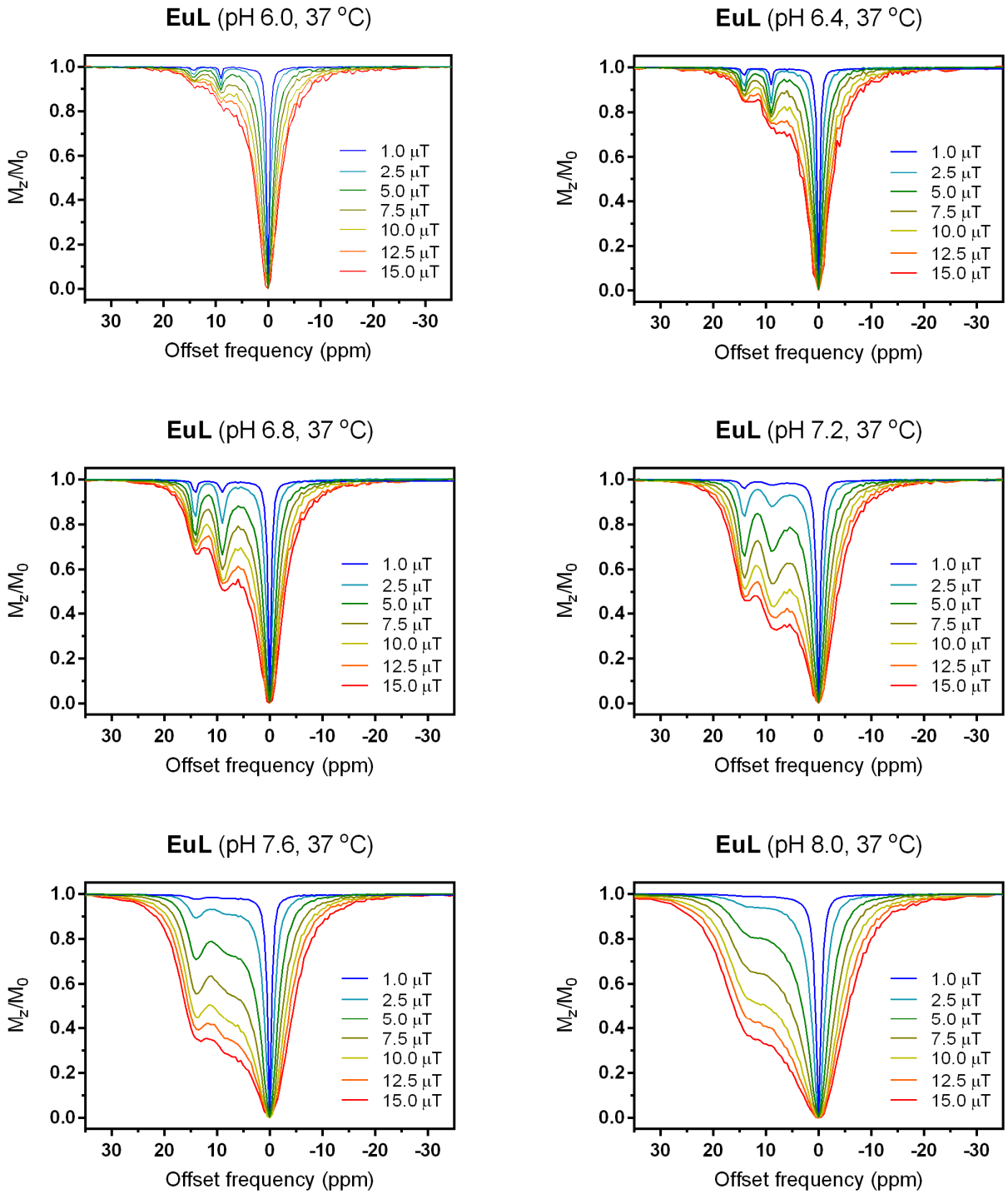

Figure S8. Z-spectra of **EuL** (5 mM in PBS) at variable pH and B_1 fields, irradiation time of 15 s and 37 °C.

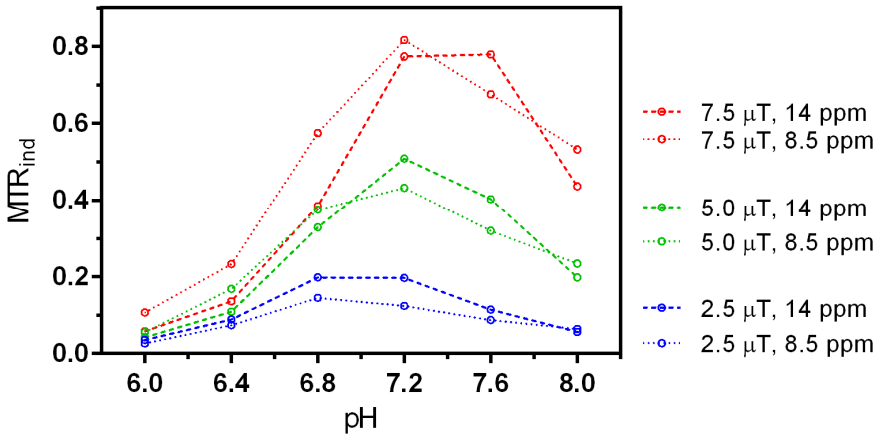

Figure S9. MTR_{ind} as a function of pH (5 mM **EuL** in PBS, 37 ^{o}C).

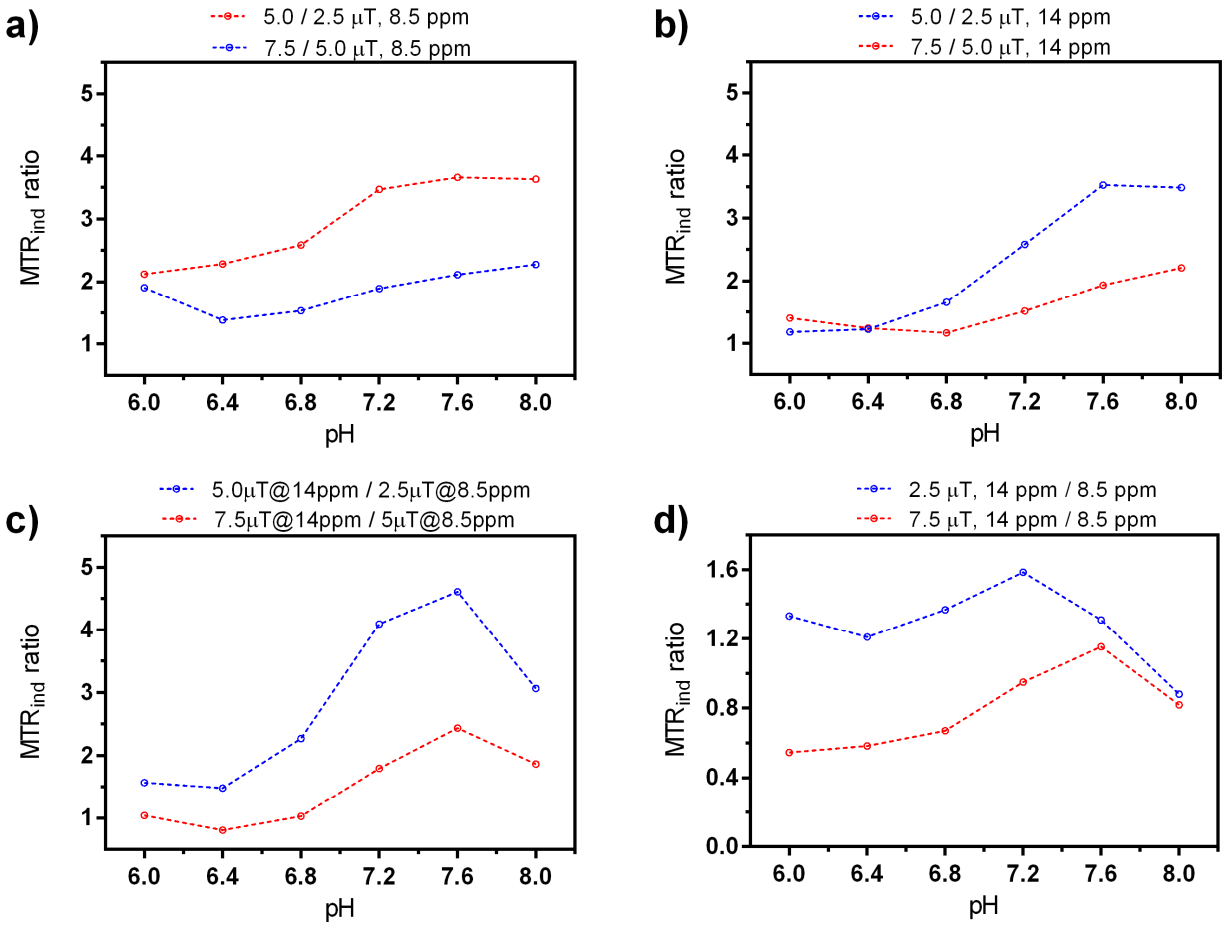

Figure S10. Ratio of MTR_{ind} for **EuL** (5 mM in PBS, 37 ^{o}C, NMR spectrometer) at varying pH values: a) signals obtained at same frequency (8.5 ppm) and different B_1; b) signals obtained at same frequency (14 ppm) and different B_1; c) signals obtained at different frequencies and different B_1; d) signals obtained at different frequencies and same B_1.

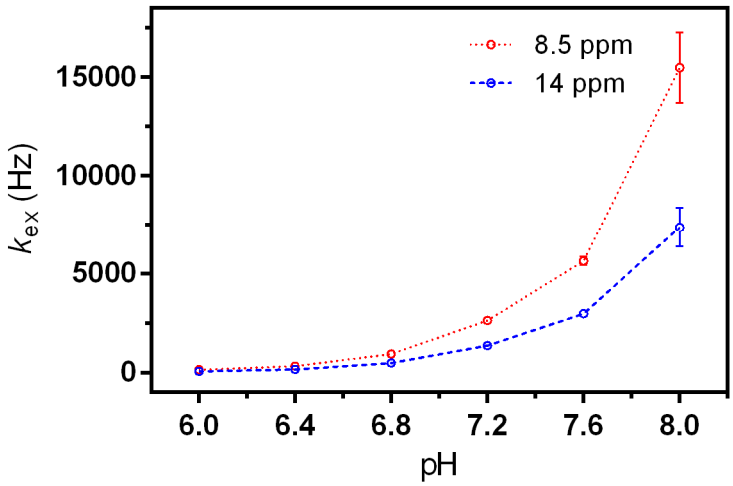

Figure S11. Exchange rate values obtained at different pH using the qCEST method (5 mM **EuL** in PBS, 37 ^{o}C).

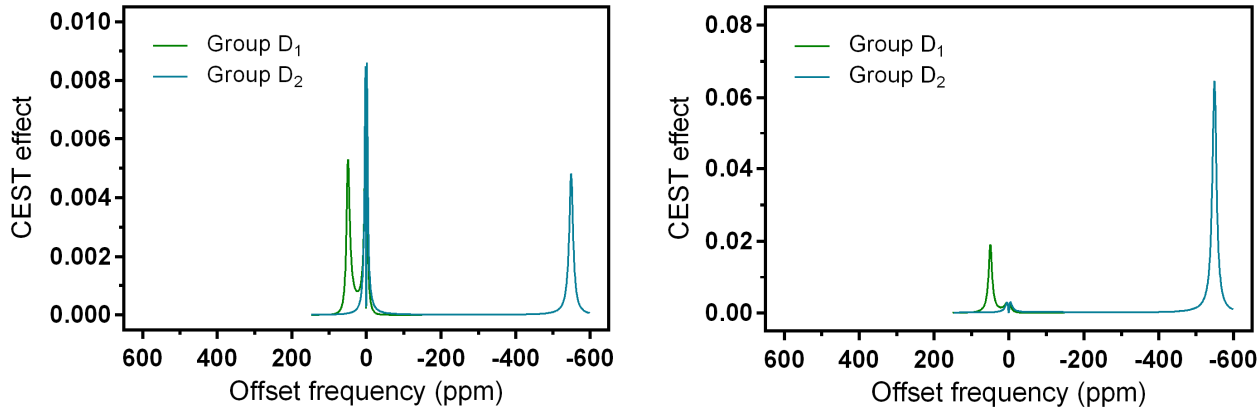

Figure S12. Simulated MTR_{asym} effects at clinical (B_1 = 5 μT, sat. time = 0.5 s, left) and preclinical settings (B_1 = 10 μT, sat. time = 5 s, right) for group D paraCEST agents.

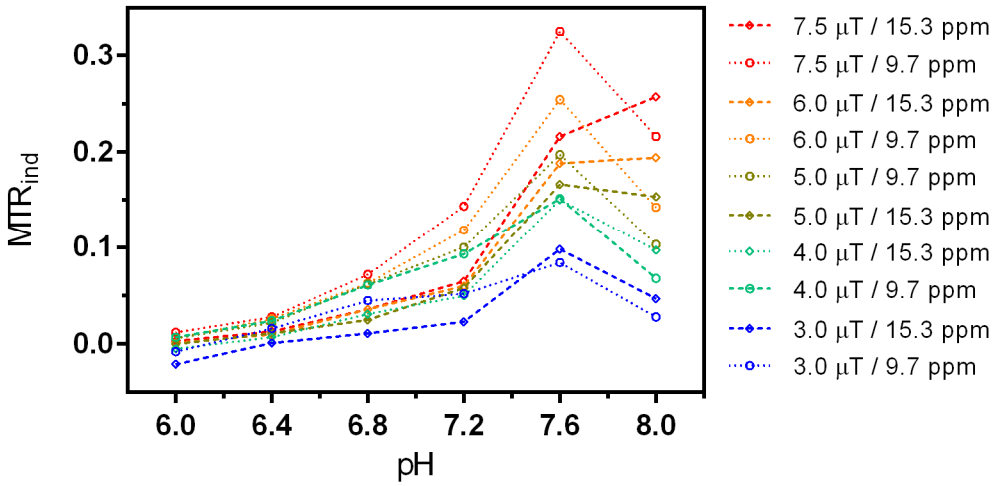

Figure S13. MTR_{ind} as a function of pH, obtained from experiments performed in the MRI scanner (3 mM **EuL** in PBS, RT).

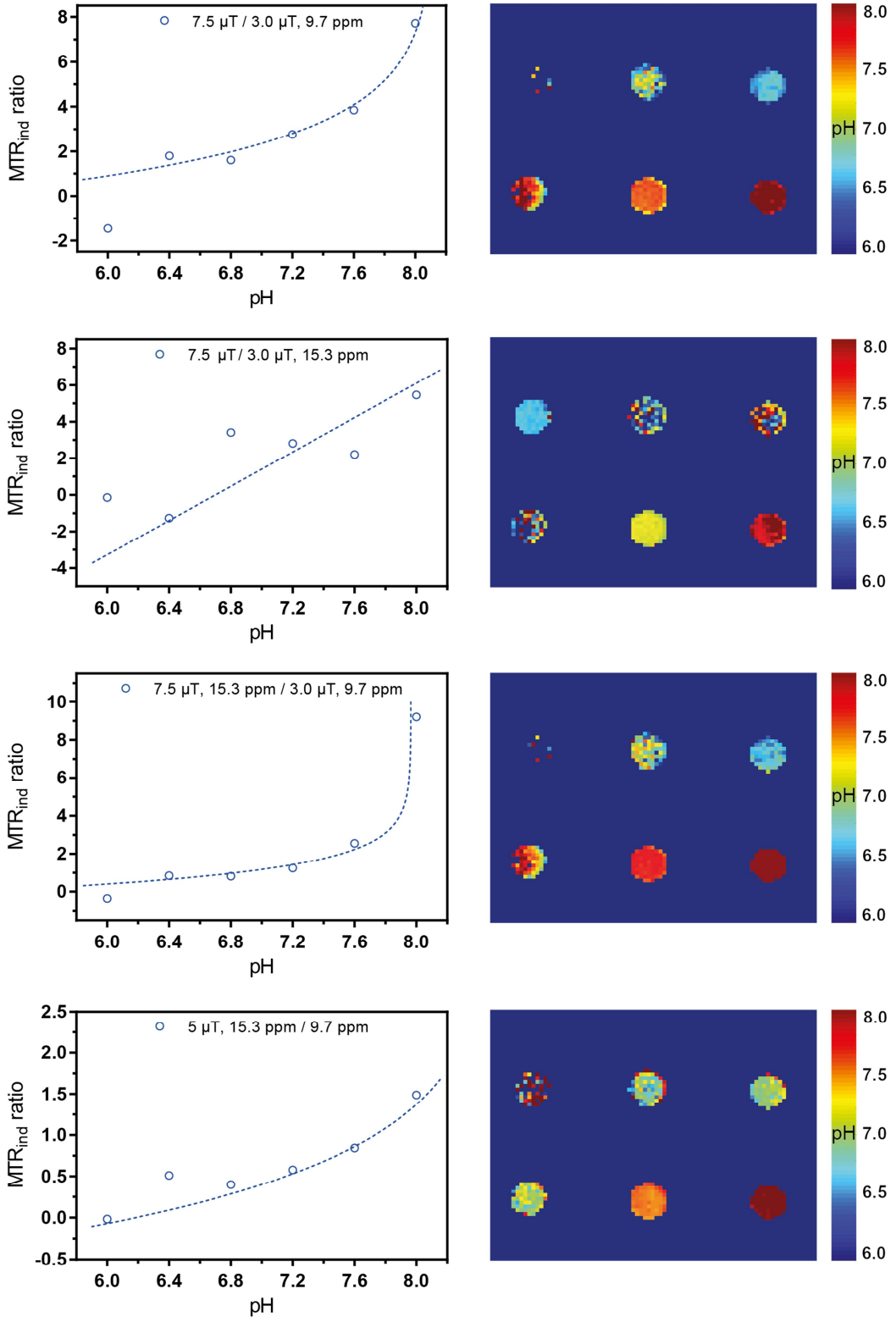

Figure S14. pH maps (right) obtained from MTR_{ind} ratio (left) on MRI tube phantoms (3 mM **EuL** in PBS, RT).

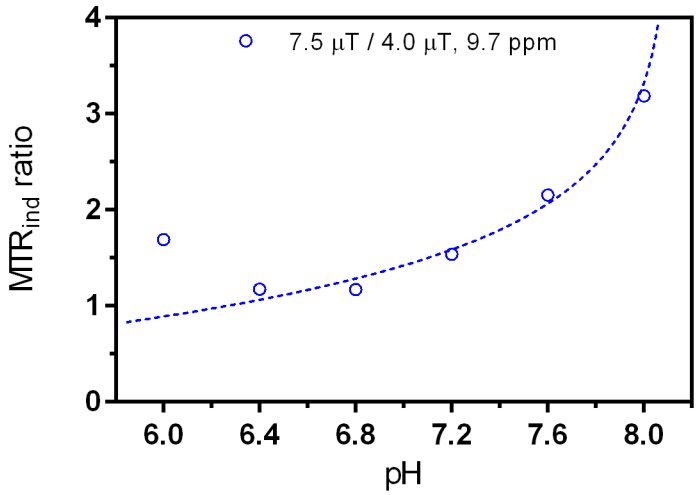

Set pH	Calc. pH
6.0 ± 0.1	–
6.4 ± 0.1	6.6 ± 0.5
6.8 ± 0.1	6.6 ± 0.2
7.2 ± 0.1	7.4 ± 0.3
7.6 ± 0.1	7.6 ± 0.1
8.0 ± 0.1	8.0 ± 0.1

Figure S15. MTR_{ind} ratio obtained from the MRI tube phantoms experiment reported in Figure 8 (left) and the table with set vs. calculated pH values from this experiment (right) (3 mM **EuL** in PBS, RT).

Supplementary Tables

Table S1. Bond distances (Å) of the metal-coordination environments observed in the X-ray structures of $[LnL]^{3+}$ complexes (Ln=Eu or Y).

Eu(1)-N(1)	2.594(15)	Y(1)-N(1)	2.568(4)
Eu(1)-N(2)	2.63(2)	Y(1)-N(2)	2.640(5)
Eu(1)-N(3)	2.644(19)	Y(1)-N(3)	2.641(5)
Eu(1)-O(1)	2.525(16)	Y(1)-N(4)	2.555(4)
Eu(1)-O(2)	2.511(15)	Y(1)-N(5)	2.652(5)
		Y(1)-N(6)	2.643(5)
		Y(1)-O(1)	2.527(4)
		Y(1)-O(2)	2.481(4)
		Y(1)-O(3)	2.445(4)
		Y(1)-O(4)	2.413(4)

Table S2. Crystal Data and Structure Refinement for the complexes.

	$[EuL](NO_3)_3 \cdot 3H_2O$	**$[YL](NO_3)_3 \cdot 3H_2O$**
formula	$C_{26}\,H_{38}\,N_{10}\,O_4\,Eu$	$C_{26}\,H_{44}\,N_{13}\,O_{16}\,Y$
mol wt	706.63	883.65
cryst syst	Monoclinic	Monoclinic
space group	C2	C2
a (Å) α (deg)	24.258(13)	25.049(5)
b (Å) β (deg)	12.124(7) 133.831(4)	11.926(5) 91.946(5)
c (Å) γ (deg)	17.312(9)	23.702(5)
V(Å^3)	3673(3)	7077(4)
Z	4	8
D(calc) (Mg/m^3)	1.278	1.659
μ (mm^{-1})	1.748	1.741
Flack param.	0.10(3)	0.243(6)
R_{int}	0.1215	0.0559
R_1[a]	0.0834	0.0569
wR_2 (all data)[b]	0.2291	0.1524

[a] $R_1 = \Sigma||F_o|-|F_c||/\Sigma|F_o|$. [b] $wR_2 = \{\Sigma[w(||F_o|^2-|F_c|^2|)^2]/\Sigma[w(F_o^4|)]\}^{1/2}$

Table S3. ^{1}H NMR shifts (D_2O, 25 ºC, pH 7.0, 400 MHz) observed for **EuL** compared to those reported previously for **EuL'**.[a)]

	H1	H2	$H3_{ax}$	$H3_{eq}$	$H4_{ax}$	$H4_{eq}$	$H5_{ax}$	$H5_{eq}$	$H6_{ax}$	$H6_{eq}$
EuL	2.45	-0.77	-9.43	-15.05	-1.62	-19.13	18.50	0.72		
EuL' [b)]	1.45	-2.18	-12.00	-17.43	-1.85	-21.20	18.74	-3.51	10.59	33.58

[a)] Structures of ligands **L** and **L'** and atom numbering is shown below.
[b)] Data for **EuL'** from the reference No. 1.

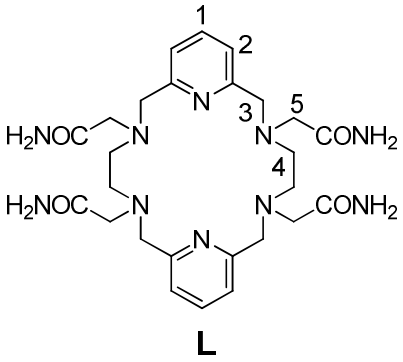

L

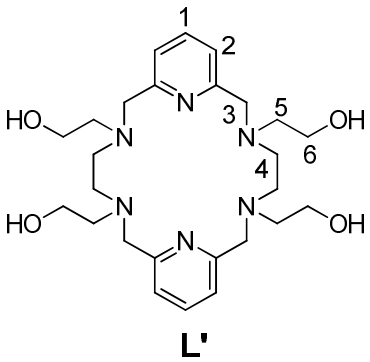

L'

Table S4. Selected paraCEST probes whose properties were used for CEST simulations.

Pos.	Group	Metal ion	Exchanging protons (#)	k_{ex} (Hz)	δ_B (ppm)	Reference
1	A	Fe^{2+}	4	400	50	2
2	A	Co^{2+}	4+4	400	68 and 102	3
3	A	Ni^{2+}	3	240-360	72-76	4
4	B	Eu^{3+}	4+4	1300 / 2600	14 / 8	This work
5	C	Tm^{3+}	4	3000	-46	5
6	C	Yb^{3+}	4+4	1100 - 1400[b)]	-15 / -18	6
7	D	Eu^{3+}	2	10000	~ 50	7-8
8	D	Tb^{3+}	2	12000[a)]	- 550	9

[a)] An estimated value for pH 7. [b)] The range of values of two amide protons at pH 7.2 and 25 ºC.

References

1. G. Castro, M. Regueiro-Figueroa, D. Esteban-Gomez, P. Perez-Lourido, C. Platas-Iglesias and L. Valencia, Magnetic Anisotropies in Rhombic Lanthanide(III) Complexes Do Not Conform to Bleaney's Theory, *Inorg. Chem.*, 2016, **55**, 3490-3497.

2. S. J. Dorazio and J. R. Morrow, Iron(II) Complexes Containing Octadentate Tetraazamacrocycles as ParaCEST Magnetic Resonance Imaging Contrast Agents, *Inorg. Chem.*, 2012, **51**, 7448-7450.

3. A. E. Thorarinsdottir, K. Du, J. H. P. Collins and T. D. Harris, Ratiometric pH Imaging with a Co^{II2} MRI Probe via CEST Effects of Opposing pH Dependences, *J. Am. Chem. Soc.*, 2017, **139**, 15836-15847.

4. A. O. Olatunde, S. J. Dorazio, J. A. Spernyak and J. R. Morrow, The NiCEST Approach: Nickel(II) ParaCEST MRI Contrast Agents, *J. Am. Chem. Soc.*, 2012, **134**, 18503-18505.

5. N. McVicar, A. X. Li, M. Suchy, R. H. E. Hudson, R. S. Menon and R. Bartha, Simultaneous In Vivo pH and Temperature Mapping Using a PARACEST-MRI Contrast Agent, *Magn. Reson. Med.*, 2013, **70**, 1016-1025.

6. S. R. Zhang, L. Michaudet, S. Burgess and A. D. Sherry, The Amide Protons of an Ytterbium(III) dota Tetraamide Complex Act as Efficient Antennae for Transfer of Magnetization to Bulk Water, *Angew. Chem. Int. Ed.*, 2002, **41**, 1919-1921.

7. Y. K. Wu, T. C. Soesbe, G. E. Kiefer, P. Y. Zhao and A. D. Sherry, A Responsive Europium(III) Chelate That Provides a Direct Readout of pH by MRI, *J. Am. Chem. Soc.*, 2010, **132**, 14002-14003.

8. Y. Wu, S. Zhang, T. C. Soesbe, J. Yu, E. Vinogradov, R. E. Lenkinski and A. D. Sherry, pH imaging of mouse kidneys in vivo using a frequency-dependent paraCEST agent, *Magn. Reson. Med.*, 2016, **75**, 2432-2441.

9. X. J. Wang, Y. K. Wu, T. C. Soesbe, J. Yu, P. Y. Zhao, G. E. Kiefer and A. D. Sherry, A pH-Responsive MRI Agent that Can Be Activated Beyond the Tissue Magnetization Transfer Window, *Angew. Chem. Int. Ed.*, 2015, **54**, 8662-8664.